JACS
JOURNAL OF THE AMERICAN CHEMICAL SOCIETY

Communication

pubs.acs.org/JACS

Two-Dimensional Superconductivity Emerged at Monatomic Bi^{2-} Square Net in Layered Y_2O_2Bi via Oxygen Incorporation

Ryosuke Sei,[†,‡] Suguru Kitani,[∥] Tomoteru Fukumura,[*,‡] Hitoshi Kawaji,[∥] and Tetsuya Hasegawa[†]

[†]Department of Chemistry, Graduate School of Science, The University of Tokyo, Tokyo 113-0033, Japan
[‡]Department of Chemistry, Graduate School of Science, Tohoku University, Sendai 980-8578, Japan
[∥]Laboratory for Materials and Structures, Tokyo Institute of Technology, Yokohama 226-8503, Japan

Supporting Information

ABSTRACT: Discovery of layered superconductors such as cuprates and iron-based compounds has unveiled new science and compounds. In these superconductors, quasi-two-dimensional layers including transition metal cations play principal role in the superconductivity via carrier doping by means of aliovalent-ion substitution. Here, we report on a two-dimensional superconductivity at 2 K in $ThCr_2Si_2$-type layered oxide Y_2O_2Bi possessing conducting monatomic Bi^{2-} square net, possibly associated with an exotic superconductivity. The superconductivity emerges only in excessively oxygen-incorporated Y_2O_2Bi with expanded inter-net distance, in stark contrast to non-superconducting pristine Y_2O_2Bi reported previously. This result suggests that the element incorporation into hidden interstitial site could be an alternative approach to conventional substitution and intercalation methods for search of novel superconductors.

Layered superconductors are a gold mine of fascinating superconductivity such as high transition temperature and unconventional pairing.[1−6] Recently, Cu intercalated Bi_2Se_3 with Bi−Se quintuple layer has been extensively studied because the strong spin−orbit coupling could be associated with topological superconductivity,[7−9] leading to possible manifestation of quantum computer. Similarly, superconducting Bi square net would provide a new platform to explore topological superconductivity, owing to the possibility of two-dimensional topological insulator.[10] So far, several layered compounds with Bi square net were reported to be superconducting.[11−13] However, the superconductivity was often subject to small superconducting volume fraction or was attributed to neighboring layer rather than Bi square net (see Table S1). $ThCr_2Si_2$-type layered compound R_2O_2Bi (R: Y, rare earth) is composed of conducting Bi^{2-} square net and insulating $(R_2O_2)^{2+}$ layer.[14] This compound can be regarded as a counterpart of $ThCr_2Si_2$ type mother compound of FeAs-based high temperature superconductor $BaFe_2As_2$[15] because of their different carrier conduction paths, Bi^{2-} square net and $(Fe_2As_2)^{2-}$ layer, respectively (Figure 1). R_2O_2Bi showed interesting properties such as chemical pressure induced metal-to-insulator transition and two-dimensional magnetotransport with the strong spin−orbit coupling[14,16] in spite of the absence of superconductivity.[6,14] In this study, we discovered two-dimensional superconductivity of Bi^{2-} square net in Y_2O_2Bi at about 2 K. It is noted that the superconductivity was not observed in pristine Y_2O_2Bi but induced by expanding inter-net distance through excessive O incorporation into hidden interstitial site. This result indicates an important role of enhanced two-dimensionality of Bi^{2-} square net in emergence of the superconductivity and provides new chemical approach to explore the superconductivity in layered compounds.

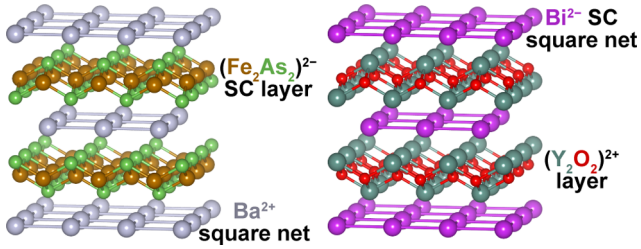

Figure 1. Crystal structures of $ThCr_2Si_2$-type $BaFe_2As_2$ (left) and Y_2O_2Bi (right). SC: superconducting.

Y_2O_2Bi was synthesized as follows. The starting materials were Bi (99.9%), Y (99.9%), and Y_2O_3 (99.9%) powders. The Y_2O_3 powder was heated at 350 °C for 1 day before use in order to eliminate absorbed moisture. Nominal amount of $Y_2O_{1+0.1n}Bi_{1.5}$ (n: integer, $1 \le n \le 10$) mixed powders were pressed into pellets by ∼5 MPa and covered with Ta foil. We denoted the samples by using indices A−J instead of n (Table S2). The excess amount of Bi was added in order to compensate volatile Bi and remove burnable Y residue in air by forming YBi.[17] This operation was performed in Ar-filled glovebox. The pellets were heated in evacuated quartz tubes at 500 °C for 7.5 h, followed by heating at 1000 °C for 20 h. The products were ground in the glovebox, pressed into pellets in air by ∼30 MPa, covered with Ta foil, and heated in evacuated quartz tubes at 1000 °C for 10 h. Crystal structures were evaluated by powder X-ray diffraction (XRD) using Cu Kα radiation (D8 DISCOVER, Bruker AXS). Rietvelt refinements were performed by RIETAN-FP,[18] and the crystal structures were drawn by VESTA.[19] Magnetic properties were measured by superconducting quantum interference device magnetometer (MPMS, Quantum Design). Electrical transport properties were evaluated by standard four-probe method (PPMS, Quantum Design). Specific heat measurements were conducted by the thermal relaxation method using a homemade

Received: May 23, 2016
Published: August 19, 2016

DOI: 10.1021/jacs.6b05275
J. Am. Chem. Soc. 2016, 138, 11085−11088

calorimeter with a ^{3}He/^{4}He dilution refrigerator.[20] Out-of-plane and in-plane magnetic field (H) direction was defined to be H parallel to and normal to the pellet surface, respectively, because of the preferential c-axis orientation (Supporting Information, SI-3).

Figure 2 shows powder XRD patterns of all samples A–J in this study (Table S2). Most of diffraction peaks were assigned as

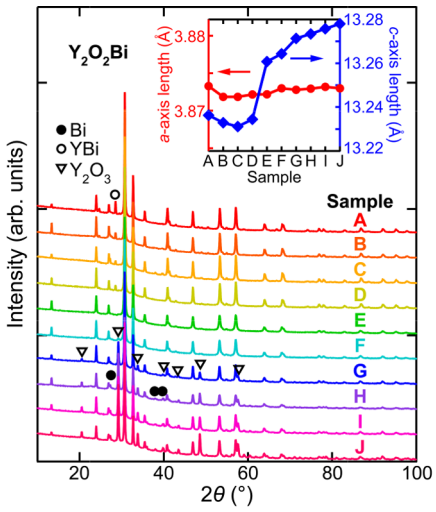

Figure 2. XRD patterns of Y_2O_2Bi samples A–J. Inset shows lattice constant of each sample. Results of the Rietveld refinements are seen in Table S2 and Figure S1.

$ThCr_2Si_2$-type Y_2O_2Bi phase, while several nonsuperconducting minor phases appeared depending on prescribed amount of O; YBi for reductive condition (samples A–D) and Y_2O_3 for oxidative condition (samples E–J) (Figure S2). The typical atomic ratio of Y/Bi in Y_2O_2Bi phase was almost stoichiometric, e.g., 2.02 for both reductive (sample B) and oxidative (F) conditions, evaluated by inductively coupled plasma mass spectroscopy and Rietveld refinement. The lattice constants for samples A–D were similar to those of Y_2O_2Bi polycrystalline powder (a = 3.8734, c = 13.2469 Å)[14] (inset of Figure 2), indicating their ideal composition. The c-axis showed abrupt expansion for sample E followed by gradual increase with almost constant a-axis toward sample J (inset of Figure 2). This expansion was possibly caused by O incorporation between Bi^{2-} square net and adjacent Y termination layers implied by jump of those distance from samples D to E in contrast with continuously changed distance between Y termination layer and adjacent O layer (Figure S3). This incorporation into hidden interstitial site is essentially different from conventional intercalation into van del Waals gap.[1,3,8,9]

Figure 3a shows the temperature dependence of magnetic susceptibility in zero-field cooling (ZFC) and field cooling (FC) at 5 Oe. No diamagnetic signal was observed for samples A–D, whereas large diamagnetic signals due to the Meissner effect were observed at about 2 K for samples E–J corresponding to the superconducting transition. The critical temperature T_c was monotonically increasing function of nominal amount of O for samples E–J. The magnetization curve at 2 K for sample I indicated the type-II superconductivity with a lower critical magnetic field of 18 Oe deduced from the magnetization minimum (inset of Figure 3a). Shielding volume fractions calculated from the magnetization curves for samples E–J confirmed bulk superconductivity of Y_2O_2Bi (Figure 3b).[21]

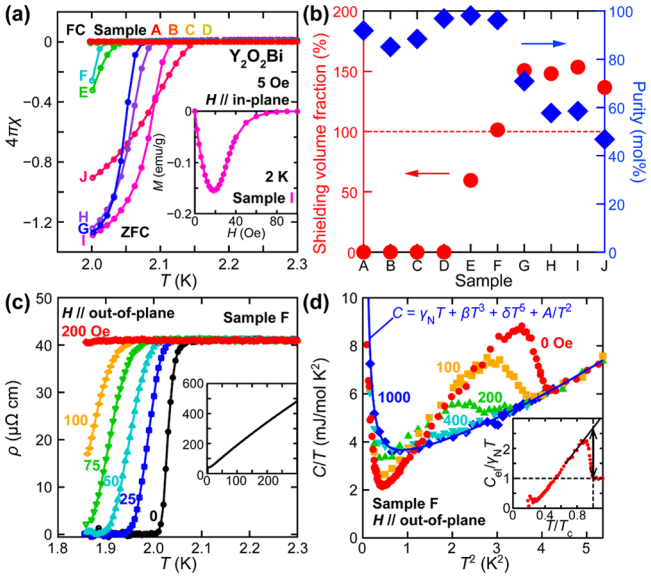

Figure 3. Superconducting properties of Y_2O_2Bi samples. (a) Temperature dependence of magnetic susceptibility with ZFC and FC process at 5 Oe for samples A–J. Inset shows magnetization curve at 2 K for sample I. (b) Evolution of shielding volume fraction and Y_2O_2Bi phase purity for samples A–J. (c) Temperature dependence of electrical resistivity near T_c and in the range of 1.85–300 K (inset) for sample F. (d) The specific heat plotted as C/T vs T^2 under various magnetic fields for sample F. Inset shows electronic contribution of specific heat C_{el} divided by $\gamma_N T$ as a function of normalized temperature T/T_c, where specific heat jump was evaluated to be $\Delta C_{el}/\gamma_N T_c$ = 1.68 (vertical arrow). T_c was derived from the electrical resistivity measurement.

Hereafter, we mainly discuss the properties of sample F because of the highest purity of Y_2O_2Bi phase (96.3 mol %) and the bulk superconductivity with sufficiently high shielding volume fraction (Figure 3b). Figure 3c shows the temperature dependence of electrical resistivity at different magnetic field. The sample showed metallic behavior (inset of Figure 3c), similar to that of a previous report.[14] Onset of superconductivity and zero-resistance at 0 Oe were observed at 2.04 and 2.01 K, respectively, and the T_c decreased with increasing magnetic field. The superconducting parameters of T_c, upper critical field H_{c2} (T = 0 K), and coherence length ξ ($H_{c2} = \Phi_0/2\pi\xi^2$; Φ_0, the flux quantum) changed monotonically for samples E–J from 2.02 K, 574 Oe, and 75.8 nm to 2.21 K, 1864 Oe, and 42.0 nm, respectively, as summarized in Figure S4 and Table S3.

Figure 3d shows the specific heat plotted as C/T vs T^2. A large jump in the specific heat was observed at T_c for each magnetic field, evidencing again the bulk superconductivity. An upturn below about 0.6 K was due to a Schottky anomaly originating from ^{209}Bi nuclei (I = 9/2). From the curve fitting of the normal state at 1000 Oe with the following equation, $C = \gamma_N T + \beta T^3 + \delta T^5 + AT^{-2}$, where $\gamma_N T$, $\beta T^3 + \delta T^5$, and AT^{-2} correspond to the electronic, phonon, and nuclear contributions, respectively; the Sommerfeld constant γ_N = 2.71 mJ mol^{-1} K^{-2}, β = 0.582 mJ mol^{-1} K^{-4}, δ = 0.0536 mJ mol^{-1} K^{-6}, and A = 0.325 mJ mol^{-1} K were obtained. From the difference in the electronic specific heat C_{el} between superconducting and normal states, the specific heat jump at T_c was evaluated to be $\Delta C_{el}/\gamma_N T_c$ = 1.68 (inset of Figure 3d), which was comparable to the Bardeen–Cooper–Schrieffer weak coupling limit 1.43 (Supporting Information, SI-2).

Electrical transport properties in Y_2O_2Bi exhibited two-dimensional superconductivity, supporting the superconducting Bi^{2-} square net. Figure 4a shows V–I curves near critical current

DOI: 10.1021/jacs.6b05275
J. Am. Chem. Soc. 2016, 138, 11085–11088

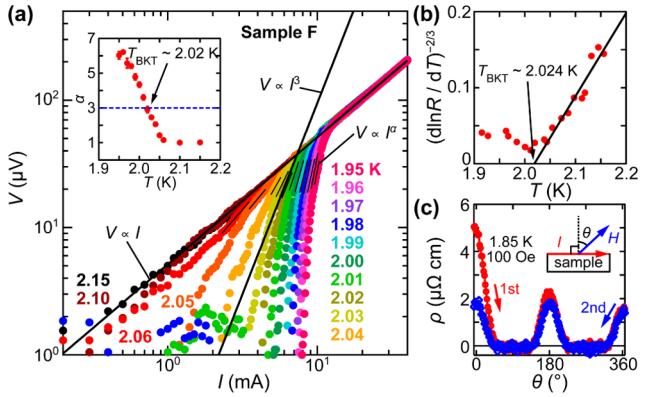

Figure 4. Two-dimensional nature of superconductivity. (a) V–I curves at various temperatures near T_c. Black lines denote the fitting result with $V \propto I^{\alpha}$ scaling law. Inset shows temperature dependence of the exponent α. (b) Temperature dependence of (d ln R/dT)$^{-2/3}$. (c) Angular-dependent magnetoresistance at 1.85 K and 100 Oe. Inset shows measurement configuration.

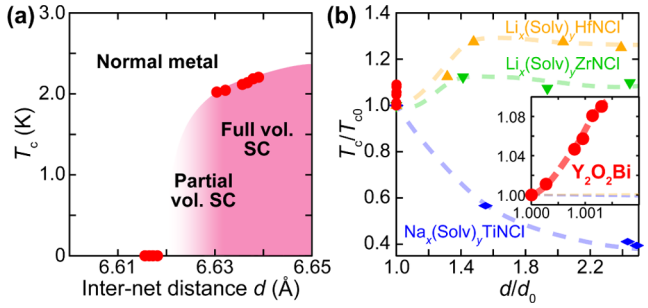

Figure 5. Evolution of superconductivity with enhancing two-dimensionality. (a) Phase diagram with T_c as a function of inter-net distance $d = c/2$. Partial and full volume superconductivity was defined from the shielding volume fraction (Figure 3b). (b) The evolution of T_c as a function of normalized Bi^{2-} inter-net and MN interlayer distance for Y_2O_2Bi and $A_x(Solv)_yMNCl$ compounds, respectively. T_{c0} and d_0 were defined from those of sample E in this study and those of Li_xHfNCl, Li_xZrNCl, and Na_xTiNCl,[31] respectively.

at around T_c. The V–I curves showed a transition of scaling law $V \propto I^{\alpha}$ above T_c from $\alpha = 1$ (ohmic law) to 3 and more with decreasing temperature. This tendency corresponded to the Berezinskii–Kosterlitz–Thouless (BKT) transition at T_{BKT} = 2.02 K as seen in inset of Figure 4a.[22,23] This value was in good coincidence with T_{BKT} independently derived from temperature dependence of resistivity according to the relationship $R(T) \propto \exp[-b(T/T_{BKT} - 1)^{-1/2}]$, in which b is the material constant (Figure 4b).[24] These results confirmed two-dimensional superconductivity of Y_2O_2Bi, indicating weak coupling between superconducting layers, i.e., Bi^{2-} square nets, as observed in cuprate[25,26] and Fe-based[27,28] superconductors. The two-dimensionality was also manifested in angular-dependent magnetoresistance as shown in Figure 4c, indicating higher H_{c2} under in-plane magnetic field (see also Figure S6b). Irreducible resistivity at $\theta = 0°$ between forward and backward sweeps might be attributed to decreased effective field due to flux pinning effect in insulating $Y_2O_2^{2+}$ layer and/or grain boundary. The appearance of the two-dimensional superconductivity is probably owing to the sufficiently high crystalline orientation of large sized crystal (Supporting Information, SI-3).

The similar shape of ρ–T curves and residual resistivity ratio irrespective to the samples ruled out the possibility of carrier doping as an effect of O incorporation (Supporting Information, SI-4). Alternative scenario is the enhanced two-dimensionality of the Bi^{2-} square net as a result of the abruptly expanded c-axis because the expansion is concomitant with the emergence of the superconductivity for samples E–J. Figure 5a shows the T_c as a function of the inter-net distance d ($d = c/2$). No superconducting signatures were observed for $d \leq 6.62$ Å except for the slight resistance-drop at about 1.9 K in the case of $d \approx 6.62$ Å (sample D in Figure S4a). The partial volume superconductivity emerged at $d = 6.63$ Å with $T_c = 2.02$ K, evidenced by small shielding volume fraction (Figure 3b) and broad resistance-drop (sample E in Figure S4a). Then, the full volume superconductivity emerged for $d > 6.63$ Å with large shielding volume fraction (Figure 3b) and sharp resistance-drop (samples F–J in Figure S4a). Here, T_c was approximately proportional to d. This result suggests that the superconductivity was induced by reducing inter-net coupling, i.e., enhancing two-dimensionality of the Bi^{2-} square net. Such tendency was scarcely seen in other superconductors,[29] except for the enhanced T_c up to about 26 K in $A_x(Solv)_yMNCl$ (A = alkali metals, Solv = organic molecules, and M = Ti, Zr, Hf) with increasing interlayer distance d between double honeycomb MN layers by intercalating organic molecules into the van del Waals gap.[3,30,31] Figure 5b shows the relative change in T_c as a function of normalized Bi^{2-} inter-net and MN interlayer distance for Y_2O_2Bi and $A_x(Solv)_yMNCl$, respectively. The T_c of Y_2O_2Bi increased much faster as a function of the normalized distance than those of $A_x(Solv)_yMNCl$ without saturation (Figure 5b), implying a peculiar feature of the superconductivity of monatomic Bi^{2-} square net.

In conclusion, we discovered the superconductivity in $ThCr_2Si_2$-type Y_2O_2Bi by increasing inter-net distance via O incorporation into hidden interstitial site without carrier doping, which would be a novel route to induce superconductivity in layered crystal. The emergent two-dimensional superconductivity of Bi^{2-} square net with strong spin–orbit coupling could be associated with exotic superconductivity like topological superconductivity, leading to possible application in quantum computer.

■ ASSOCIATED CONTENT

Supporting Information

The Supporting Information is available free of charge on the ACS Publications website at DOI: 10.1021/jacs.6b05275.

Properties of other Bi square net compounds, results of Rietveld refinement, image of O incorporation, superconducting properties of all samples, and discussion about specific heat, c-axis orientation, and carrier doping (PDF)

■ AUTHOR INFORMATION

Corresponding Author

*E-mail: tf1@tohoku.ac.jp.

Notes

The authors declare no competing financial interest.

■ ACKNOWLEDGMENTS

This research was in part supported by Core Research for Evolutionary Science and Technology of Japan Science and Technology Agency and JSPS KAKENHI (26600091, 26105002).

DOI: 10.1021/jacs.6b05275
J. Am. Chem. Soc. 2016, 138, 11085–11088

REFERENCES

(1) Klemm, R. A., Ed. *Layered Superconductors*; Oxford Univ. Press: Oxford, 2012; Vol. *1*.
(2) Bednorz, J. G.; Müller, K. *Z. Phys. B: Condens. Matter* **1986**, *64*, 189−193.
(3) Yamanaka, S.; Hotehama, K.; Kawaji, H. *Nature* **1998**, *392*, 580−582.
(4) Mackenzie, A. P.; Maeno, Y. *Rev. Mod. Phys.* **2003**, *75*, 657−712.
(5) Kamihara, Y.; Watanabe, T.; Hirano, M.; Hosono, H. *J. Am. Chem. Soc.* **2008**, *130*, 3296−3297.
(6) Hosono, H.; Tanabe, K.; Takayama-Muromachi, E.; Kageyama, H.; Yamanaka, S.; Kumakura, H.; Nohara, M.; Hiramatsu, H.; Fujitsu, S. *Sci. Technol. Adv. Mater.* **2015**, *16*, 033503−1−87.
(7) Qi, X.-L.; Zhang, S.-C. *Rev. Mod. Phys.* **2011**, *83*, 1057−1110.
(8) Hor, Y. S.; Williams, A. J.; Checkelsky, J. G.; Roushan, P.; Seo, J.; Xu, Q.; Zandbergen, H. W.; Yazdani, A.; Ong, N. P.; Cava, R. J. *Phys. Rev. Lett.* **2010**, *104*, 057001.
(9) Sasaki, S.; Kriener, M.; Segawa, K.; Yada, K.; Tanaka, Y.; Sato, M.; Ando, Y. *Phys. Rev. Lett.* **2011**, *107*, 217001.
(10) Luo, W.; Xiang, H. *Nano Lett.* **2015**, *15*, 3230−3235.
(11) Mizoguchi, H.; Matsuishi, S.; Hirano, M.; Tachibana, M.; Takayama-Muromachi, E.; Kawaji, H.; Hosono, H. *Phys. Rev. Lett.* **2011**, *106*, 057002.
(12) Han, F.; Malliakas, C. D.; Stoumpos, C. C.; Sturza, M.; Claus, H.; Chung, D. Y.; Kanatzidis, M. G. *Phys. Rev. B: Condens. Matter Mater. Phys.* **2013**, *88*, 144511.
(13) Vinod, K.; Bharathi, A.; Satya, A. T.; Sharma, S.; Devidas, T. R.; Mani, A.; Sinha, A. K.; Deb, S. K.; Sridharan, V.; Sudar, C. S. *Solid State Commun.* **2014**, *192*, 60−63.
(14) Mizoguchi, H.; Hosono, H. *J. Am. Chem. Soc.* **2011**, *133*, 2394−2397.
(15) Rotter, M.; Tegel, M.; Johrendt, D. *Phys. Rev. Lett.* **2008**, *101*, 107006.
(16) Sei, R.; Fukumura, T.; Hasegawa, T. *ACS Appl. Mater. Interfaces* **2015**, *7*, 24998−25001.
(17) The nominal amount of Bi was changed to 1.8, 1.7, and 1.6 for A, B, and C, respectively, in order to compensate for increased Y residue.
(18) Izumi, F.; Momma, K. *Solid State Phenom.* **2007**, *130*, 15−20.
(19) Momma, K.; Izumi, F. *J. Appl. Crystallogr.* **2011**, *44*, 1272−1276.
(20) Kohama, Y.; Tojo, T.; Kawaji, H.; Atake, T.; Matsuishi, S.; Hosono, H. *Chem. Phys. Lett.* **2006**, *421*, 558−561.
(21) The shielding volume fraction over 100% was caused by the polycrystalline nature of the samples.
(22) Berezinskii, Z. L. *Sov. Phys. JETP* **1971**, *32*, 493−500.
(23) Kosterlitz, J. M.; Thouless, D. J. *J. Phys. C: Solid State Phys.* **1973**, *6*, 1181−1203.
(24) Halperin, B. I.; Nelson, D. R. *J. Low Temp. Phys.* **1979**, *36*, 599−616.
(25) Yeh, N.-C.; Tsuei, C. C. *Phys. Rev. B: Condens. Matter Mater. Phys.* **1989**, *39*, 9708−9711.
(26) Li, Q.; Hücker, M.; Gu, G. D.; Tsvelik, A. M.; Tranquada, J. M. *Phys. Rev. Lett.* **2007**, *99*, 067001.
(27) Schneider, R.; Zaitsev, A. G.; Fuchs, D.; von Löhneysen, H. *J. Phys.: Condens. Matter* **2014**, *26*, 455701.
(28) Lin, Z.; Mei, C.; Wei, L.; Sun, Z.; Wu, S.; Huang, H.; Zhang, S.; Liu, C.; Feng, Y.; Tian, H.; Yang, H.; Li, J.; Wang, Y.; Zhang, G.; Lu, Y.; Zhao, Y. *Sci. Rep.* **2015**, *5*, 14133−1−9.
(29) In the case of ionic and molecular intercalation into van der Waals gap as reported in graphite, chalcogenides, nitride halides, and so on, carrier doping or intercalated components were essential to induce the superconductivity (Chapter 2 in ref 1), rather than increased interlayer distance.
(30) Takano, T.; Kishiume, T.; Taguchi, Y.; Iwasa, Y. *Phys. Rev. Lett.* **2008**, *100*, 247005.
(31) Kasahara, Y.; Kuroki, K.; Yamanaka, S.; Taguchi, Y. *Phys. C* **2015**, *514*, 354−367.

DOI: 10.1021/jacs.6b05275
J. Am. Chem. Soc. 2016, 138, 11085−11088